Electronic Supplementary Material (ESI) for Physical Chemistry Chemical Physics

Supporting information

Structure and bonding of the gold-subhalide cluster *I*-$Au_{144}Cl_{60}^{[z]}$

Alfredo Tlahuice-Flores,* David Black, Stephan B. H. Bach, Miguel José-Yacamán, Robert L. Whetten*

Department of Physics and Astronomy, University of Texas at San Antonio, One UTSA Circle, San Antonio, TX, 78249.

email: Robert.Whetten@utsa.edu, tlahuicef@gmail.com

Electronic Supplementary Material (ESI) for Physical Chemistry Chemical Physics

PART I

EXPERIMENTAL METHODS AND MATERIALS

A. METHODS

The ESI-MS method employed follows essentially the procedure described by Tracy et al.[1] except that infusion without electrolyte (cesium acetate) was used to observe the high charge-state [4+] of the Cs-free clusters. [The cluster samples were synthesized and characterized separately as described in the main text's Reference 13.]

Briefly, we electrosprayed the analyte (clusters) out of 50:50 methanol-toluene. In the methanol was typically dissolved 100-mM cesium acetate (hereafter 'electrolyte'). In the toluene was dissolved ~ 1-mM of the cluster sample (hereafter simply 'analyte'). So when the two solutions are combined 1:1, the working solution is 50 mM electrolyte and 0.5 mM analyte. Although these concentrations are those described in Ref. 1 for Au_{25} clusters, they worked well to identify the signal at expected parent ion mass-to-charge ratios for the massive species described here, after which the concentrations were adjusted (as described below).

The instrument is a commercial electrospray ionization time-of-flight mass spectrometer (ESI-ToF-MS), namely Bruker 'MicroToF', prior to the ToF analyzer. [It has a hexapole ion guide for ion focusing prior to the 'pusher' of the ToF.] For all these measurements, the instrument was optimized iteratively to high-mass operation using cesium-triiode (in methanol) which forms clusters ranging to m/z > 10,000. To obtain the higher m/z ions it is important to increase the hexapole's radiofrequency (RF) voltage to its maximum value (800-V peak-to-peak).

Under the described conditions, the distribution of detected ions (various charge-states and degrees of Cs-ion attachment) appears rather similar to that published previously by Qian and Jin,[3] wherein $Au_{144}(peth)_{60}$ species were identified in the [2+] and [3+] charge-states and the Cs-ion numbers peaked at 3 or 4 attached ions. Under these conditions, the low-mass range is dominated by a long series of peaks attributable to electrolyte clusters.

To obtain the results shown in *Fig. 2*, one infuses without cesium acetate but with all other ESI-MS instrumental and solution conditions identical. In practice, this means that the operating conditions are first established as above, then rinsed with electrolyte-free solution, and finally replaced this by analyte solution to which no electrolyte had been added. Generally, repeated analyses on various days by the same operator (DB) demonstrate that some persistence and care is required to establish the conditions whereby the mass spectra have the signal-to-noise evident in *Fig. 2*.

The main panel of *Figure 2* shows the mass spectrum obtained with electrolyte-free infusion over a wide range of m/z, < 7 to > 13 kDa/z, which encompasses the expected m/z for the $Au_{144}(peth)_{60}$ species in the z = 3+ to 5+ charge-states. At the low end, the elimination of the electrolyte-cluster signal (see above) allows the features indicated to be prominently identified. Beyond the high end, the [2+] features are also strongly reduced.

The principal species are identified as indicated by the labels in this main panel: the $(144,60)^{[3+,4+]}$ ions, along with the ions attributable to a reaction byproduct (130,50) in the same two charge-states.[2] The inset panel contains expanded views of the regions selected to show the assignment of the charge-states and the shapes of the peaks, consistent with natural isotopic abundances. Minor features are attributed to expected fragments and slight contamination by residual electrolyte.[3,4] Note that [5+] ions are not detected at all.

PART II

THEORETICAL METHODS

We use a theoretical approach based on Density Functional Theory (DFT) to perform the structural relaxation of the $Au_{144}(SR)_{60}^{z}$ clusters based on Lopez-Acevedo *et al.* model[5] and the Pd_{145} structure by Dahl.[6] The proposed initial structures held a perfect *I* symmetry (with an I_h core for structure derivates from Dahl cluster) and were considered relaxed when a 0.01 eV/Å value in force was obtained. The methodology of the optimization stage used a double-ζ polarized basis set, the Perdew-Burke-Ernzehorf (PBE)[7] parametrization for the exchange-correlation functional, within the generalized gradient approximation (GGA), and a Troullier Martins scalar relativistic norm-conserving pseudopotentials[8] as implemented in the SIESTA package[9]. In the case of the -SH ligand, during the optimization stage, hydrogens bound to the sulphur atoms orientate on *trans* positions but *I* symmetry was maintained as can be verified by applying a 0.1 Å tolerance in position of the Cartesian coordinates.

REFERENCES

(1) Tracy, J. B.; Crowe, M. C.; Parker, J. F.; Hampe, O.; Fields-Zinna, C. A.; Dass, A.; Murray, R. W. *J. Am. Chem. Soc*. **2007**, 129, 16209–17215.

(2) Chaki, N. K.; Negishi, Y.; Tsunoyama, H.; Shichibu, Y.; Tsukuda, T. *J. Am. Chem. Soc*. **2008**, 130, 8608–8610.

(3) Qian, H.; Jin, R. *Nano Lett.* **2009**, *9*, 4083-4087.

(4) C. A. Fields-Zinna, R. Sardar, C. A. Beasley and R. W. Murray. *J. Am. Chem. Soc.*, **2009**,131, 16266.

(5) Lopez-Acevedo, O.; Akola, J.; Whetten, R. L.; Grönbeck, H.; Häkkinen, H. *J. Phys. Chem. C* **2009**, 113, 5035.

(6) Tran, N. T.; Powell, D. R.; Dahl, L. F. *Angew. Chem., Int. Ed*. **2000**, 39, 4121– 4125.

(7) Perdew, P.; Burke, K.; Ernzerhof, M. *Phys. Rev. Lett.* **1996**, 77, 3865-3868.

(8) Troullier, N.; Martins, J. L. *Phys. Rev. B* **1991**, 43, 1993-2006.

(9) Soler, J. M.; Artacho, E.; Gale, J. D.; García, A.; Junquera, J.; Ordejón, P.; Sánchez-Portal, D. *J. Phys.: Condens. Matter* **2002**, 14, 2745-2779.

Ref 13 in manuscript: Bahena, D.; Bhattarai, N.; Santiago, U.; Tlahuice, A.; Ponce, A.; Bach, S.B. H.; Yoon B.; Whetten, R. L.; Landman, U.; Jose-Yacamán, M. J. Phys. Chem. Lett., 2013, 4, 975–981.

PART III

Tables S1 and S2. Analysis of the point group of the Au_{144} clusters.

$Au_{144}Cl_{60}^{[z]}$	Tolerance (Å)	Point group
Neutral, z = 0	0.12 0.13	C_2 I
Dication, z = 2 0.14 eV more stable than I_h core one (from Dahl structure)	0.04 **0.043**	C_2 ***I***
Tetra-cation z = 4	0.041 **0.043**	D_5 *I*

$Au_{144}(SH)_{60}^{[z]}$	Tolerance (Å)	Point group
Neutral (z=0)	0.05 0.07 0.094	C_2 D_2 I
Spin polarized (z = 0)	0.048 0.068 0.11	C_2 D_2 I
Dication (z = 2)	0.001 0.01 0.035 **0.036**	C_1 C_1 D_5 ***I***

In both tables are given the small tolerance in position in order to obtain an *I* symmetry.

PART IV

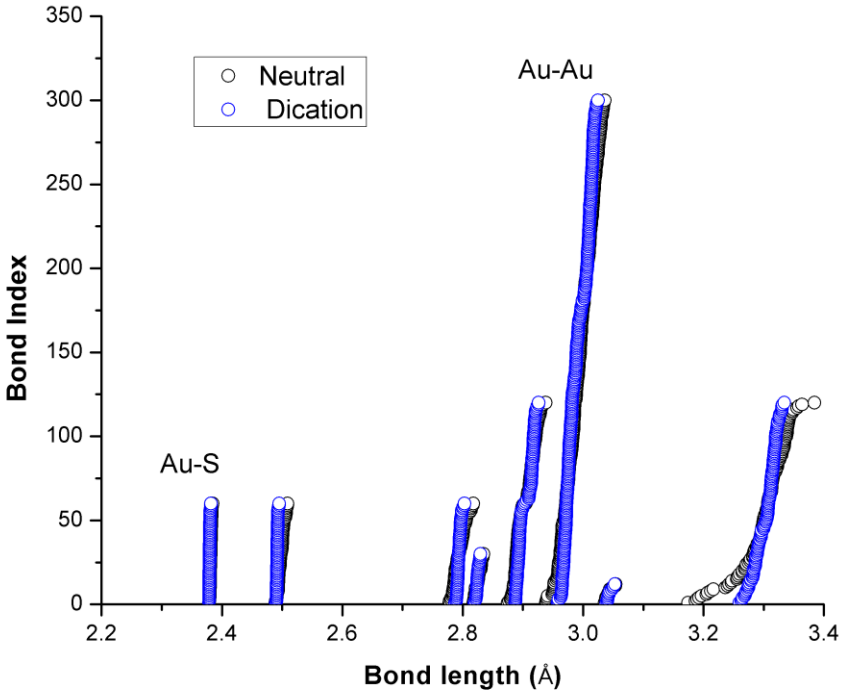

Figure S1. Bond lengths of the $Au_{144}(SH)_{60}^{z}$ clusters.

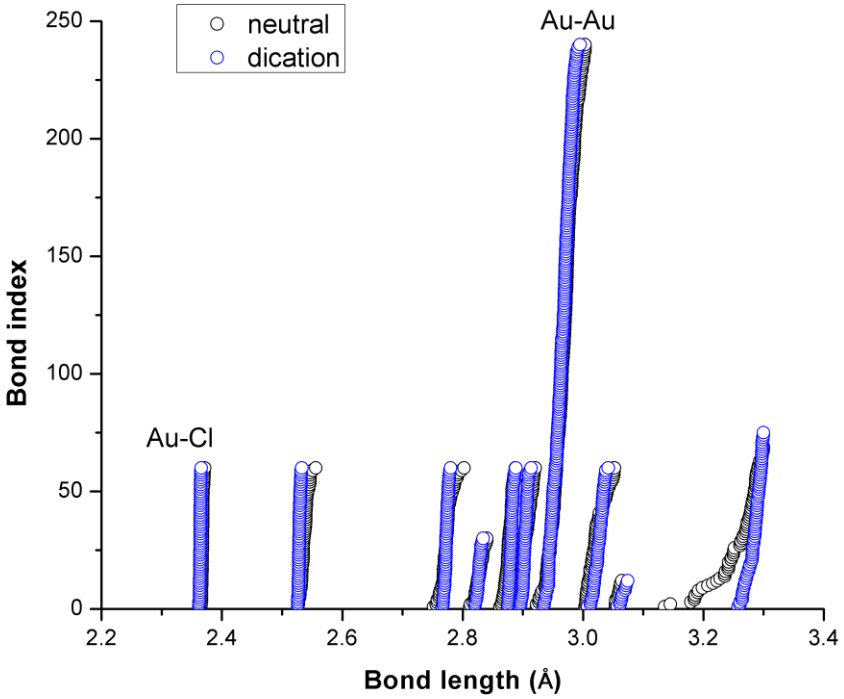

Figure S2. Bond lengths of the $Au_{144}(Cl)_{60}^{z}$ clusters.

PART V

Table S3. Frontier orbitals of Au_{25} and Au_4 clusters.

Cluster	HOMO-LUMO gap, eV	HOMO levels, eV	LUMO levels, eV
$Au_{25}Cl_{18}^-$ (***T_h*** point group)	1.18	-3.51, -3.51, -3.51	-2.33, -2.33
$Au_{25}(SCH_3)_{18}^-$ (C_i)	1.32	-2.32 -2.32 -2.28	-0.96 -0.92
Au_4Cl_4 (D_{2d})	3.42	-5.83 -5.83	-2.41
Au_4 $(SCH_3)_4$ (D_{2d})	4.6	-5.32	-0.72

Results shown in Table S3 are in agreement with Table 3 of references: D.-E. Jiang, M. Walter, *Nanoscale* **2012**, 4, 4234-4239.

Table S4. Frontier orbitals of Au_{144} clusters.

Cluster	HOMO-LUMO gap, eV	HOMO levels, eV	LUMO levels, eV
$Au_{144}(SH)_{60}$ neutral	0.10	-3.73 -3.70	-3.69 -3.68 -3.67
Spin polarized	0.03	-3.73	-3.70 -3.69 -3.68 -3.67
$Au_{144}(SH)_{60}$ dication	0.12	-5.17	-5.05 -5.05 -5.05 -5.04 -5.04
$Au_{144}Cl_{60}$ neutral	0.04	-4.56	-4.52 -4.51 -4.51 -4.49
$Au_{144}Cl_{60}$ dication	0.2	-5.17	-4.97 -4.97 -4.96 -4.96 -4.96

It is evident from Table S4 that $Au_{144}Cl_{60}$ with [2+] charge holds more degenerate electronic levels indicating a more symmetric structure. In the [4+] state, the HOMO is 5-fold degenerate (-6.00 eV) and the LUMO is non-degenerate (-5.64 eV), such that the gap is +0.36 eV.

PART VI

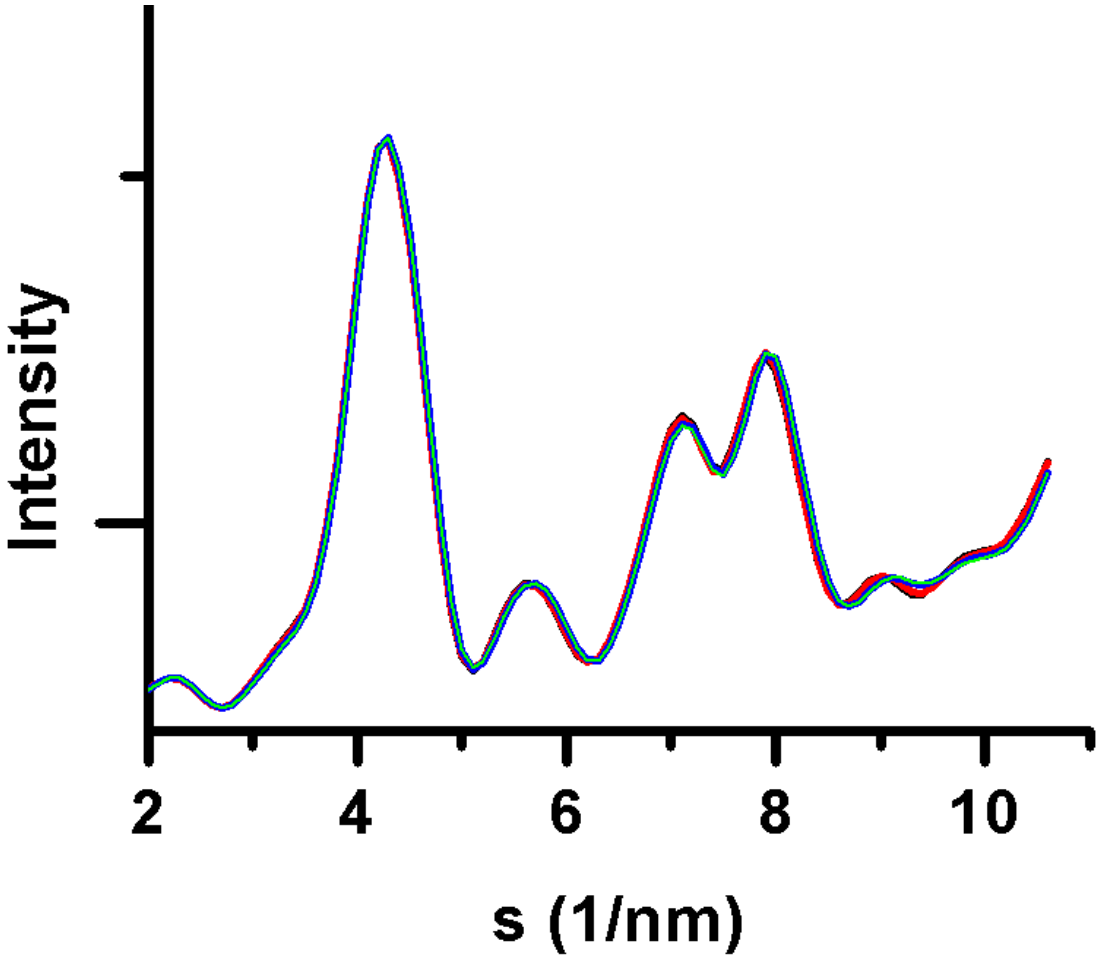

Figure S4. Calculated structure-factors (relating to XRD diffraction patterns) of the Au_{144} clusters.

The colours denote: (black) $Au_{144}(SH)_{60}^{[0]}$; (red) $Au_{144}(SH)_{60}^{[2+]}$; (blue) $Au_{144}Cl_{60}^{[0]}$; (green) $Au_{144}Cl_{60}^{[2+]}$.

The good overlap emphasizes that, at low resolution, the ordering is common to all structures examined.

PART VII

Table S4. Point group analysis of the various shells of the relaxed $Au_{144}Cl_{60}^{[2+]}$ with initial I_h core (Pd_{145})

Cluster	Tolerance (Å)	Point group
$Au_{144}Cl_{60}^{[2+]}$	0.032	C_3
With initial I_h core	0.033	T
	0.034	I (it never holds I_h)
Au_{114}	0.025	C_2
	0.028	D_5
	0.035	I
	0.42	I_h
Au_{54}	0.016	C_2
	0.019	D_5
	0.021	I
	0.023	I_h
Au_{60}	0.027	C_2
	0.028	D_5
	0.034	I
	0.42	I_h
Au_{12}	0.0037	Ci
	0.0069	C_{2h}
	0.0079	D_{2h}
	0.0088	I_h
Au_{42}	0.015	C_2
	0.02	D_5
	0.021	I
	0.023	I_h
Cl_{60}	0.03	C_2
	0.031	T
	0.033	I

PART VIII

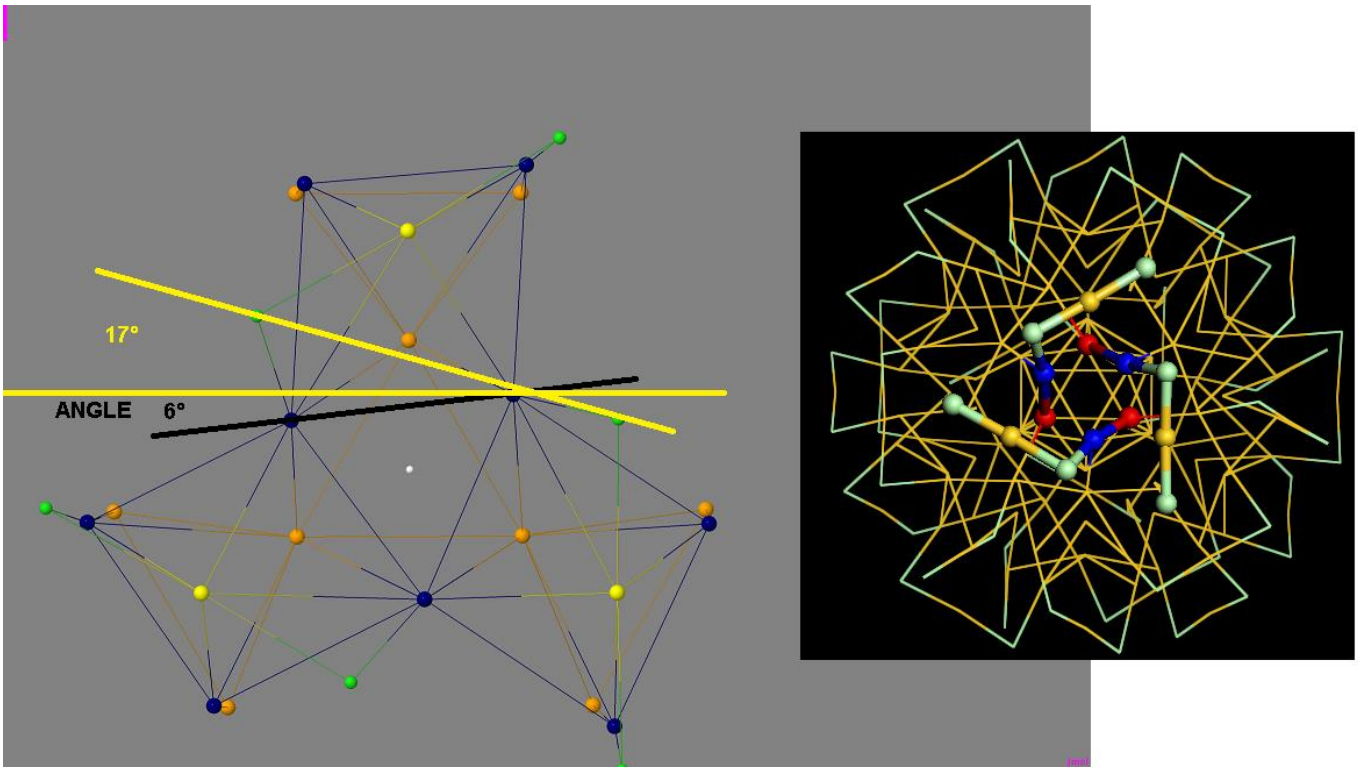

Figure S5. Determination of the special angles in the $Au_{144}Cl_{60}$ $^{[4+]}$ cluster.

PART IX

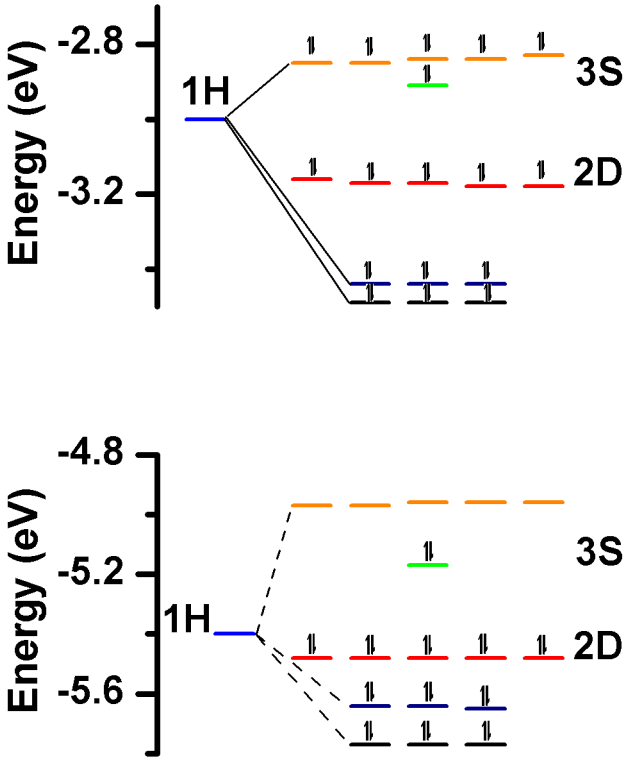

Figure S6. Energy level diagrams, as in Fig. 2, showing the occupancy of the orbitals of the $Au_{144}Cl_{60}$ $^{[z]}$, as optimized in charge states [8-] (above) and [2+] (below).

PART X

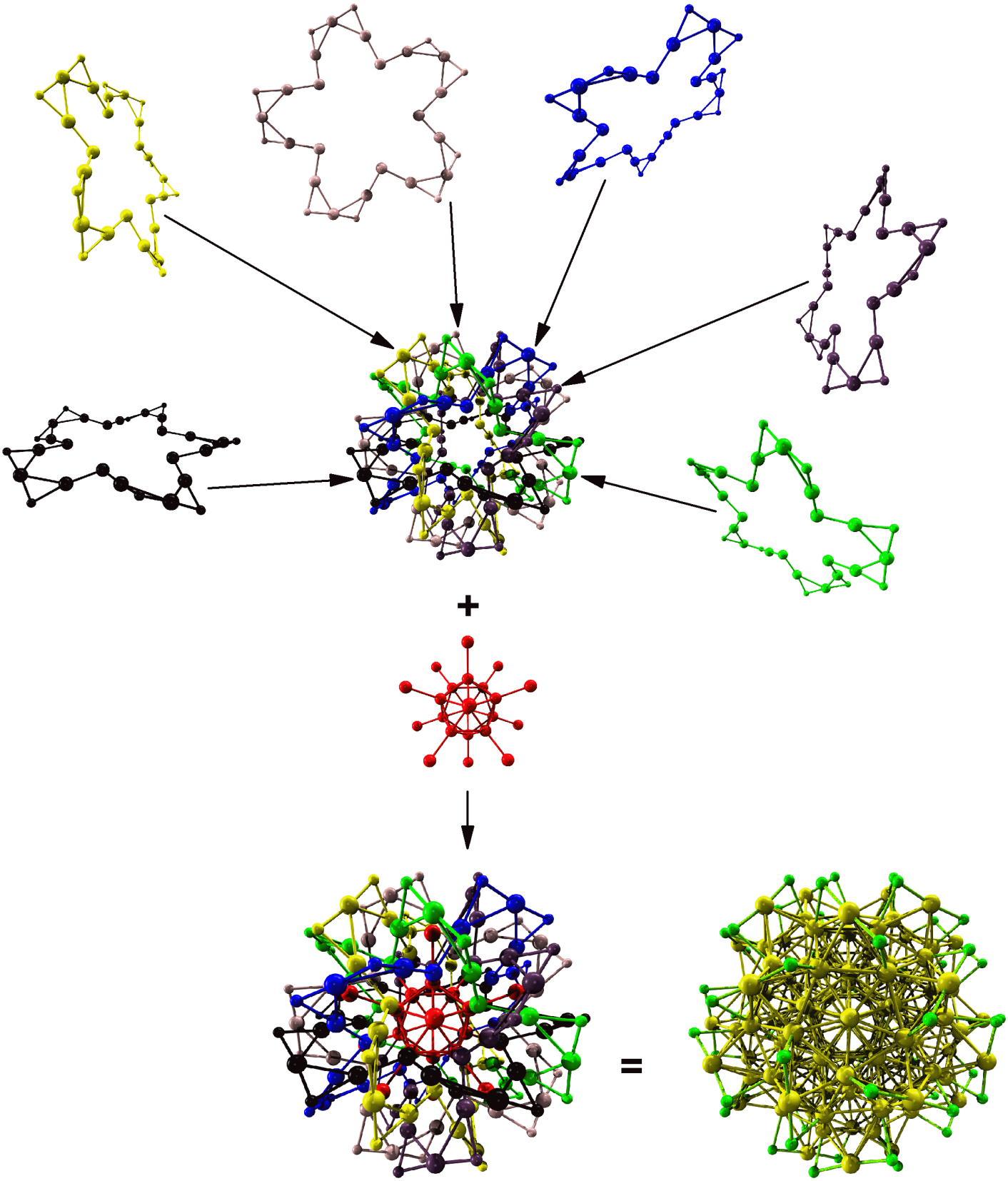

Figure S7. $Au_{144}Cl_{60}$ [z] cluster given as 6 strands (180 atoms) and Au_{24} cluster.